Using a multi-agent system approach for microaneurysm detection in fundus images

Carla Pereira, Diana Viega, Jason Mahdjoub, Zahia Guessoum, Luis Gonçalves, Manuel Ferreira, Joao Monteiro

Using a multi-agent system approach for microaneurysm detection in fundus images

Carla Pereira [a,*], Diana Veiga [a,b], Jason Mahdjoub [c], Zahia Guessoum [c], Luís Gonçalves [d], Manuel Ferreira [a,b], João Monteiro [a]

[a] *Centro Algoritmi, University of Minho, Campus de Azurém, 4800-058 Guimarães, Portugal*
[b] *ENERMETER, Parque Industrial Celeirós 2ªFase, Lugar de Gaião – Lotes 5/6, 4705-025 Aveleda, Braga, Portugal*
[c] *CReSTIC – MODECO, University of Reims, Rue des Crayères, 51100 Reims, France*
[d] *Oftalmocenter, Rua Francisco Ribeiro de Castro, nº 205, Azurém, 4800-045 Guimarães, Portugal*

Objective: Microaneurysms represent the first sign of diabetic retinopathy, and their detection is fun-damental for the prevention of vision impairment. Despite several research attempts to develop an automated system to detect microaneurysms in fundus images, none has shown the level of performance required for clinical practice. We propose a new approach, based on a multi-agent system model, for microaneurysm segmentation. *Methods and materials:* A multi-agent based approach, preceded by a preprocessing phase to allow con-struction of the environment in which agents are situated and interact, is presented. The proposed method is applied to two available online datasets and results are compared to other previously described approaches

Results: Microaneurysm segmentation emerges from agent interaction. The final score of the proposed approach was 0.240 in the Retinopathy Online Challenge.

Conclusions: We achieved competitive results, primarily in detecting microaneurysms close to vessels, compared to more conventional algorithms. Despite these results not being optimum, they are encour-aging and reveal that some improvements may be made.

1. Introduction

The presence of microaneurysms (MAs) in the retina is often the first sign of diabetic retinopathy (DR), so their early detection is crucial for the prevention of blindness. Therefore, it is of great importance to include automatic detection of MAs in a screening program. These types of lesions are commonly described as isolated, small, round objects, of 10–100 μm in diameter. In practice, they may appear as a conglomeration of more than one MA or in association with larger vessels. MAs are frequently indistinguishable from dot-hemorrhages in color fundus photographs, in which both appear red. However, these two types of lesions have the same clinical implications, so there is usually no need for an automated MA detector to distinguish between them. The number of MAs is positively correlated with the severity and progression of DR, at least in the early stages of the disease [1].

Since MAs can easily be observed in digital color fundus images and their number has clinical implications, several research attempts to develop an automated system to detect MAs have been made in recent years. However, none has shown the level of performance required for clinical practice. The primary difficulties with these algorithms lie in the low contrast between red lesions and background in fundus images, as well as the proximity of MAs to blood vessels. The algorithms often process the entire image in the same way and do not consider its local information, leading to rigid systems without the capacity to generalize. In the present study, a new approach, based on a multi-agent system (MAS), is proposed. The inclusion of MAS models in automatic medical image analysis systems is recent, and has been revealed as a research field in expansion. However, these models have already been used in the segmentation of magnetic resonance [2] and ultrasound [3] images. To the best of our knowledge, this kind of approach has been implemented by our group alone with regard to retinal blood vessel segmentation in fundus images [4].

A MAS is typically composed of a set of agents that are situated, and interact, in a virtual or real environment. In this new approach for detection of MAs in color fundus images, the environment includes an image resulting from a preprocessing step. The MA segmentation then emerges from agent interaction as a global behavior.

* Corresponding author. Tel.: +351 253 510 190.
E-mail addresses: id2723@alunos.uminho.pt, csusanacp@gmail.com (C. Pereira).

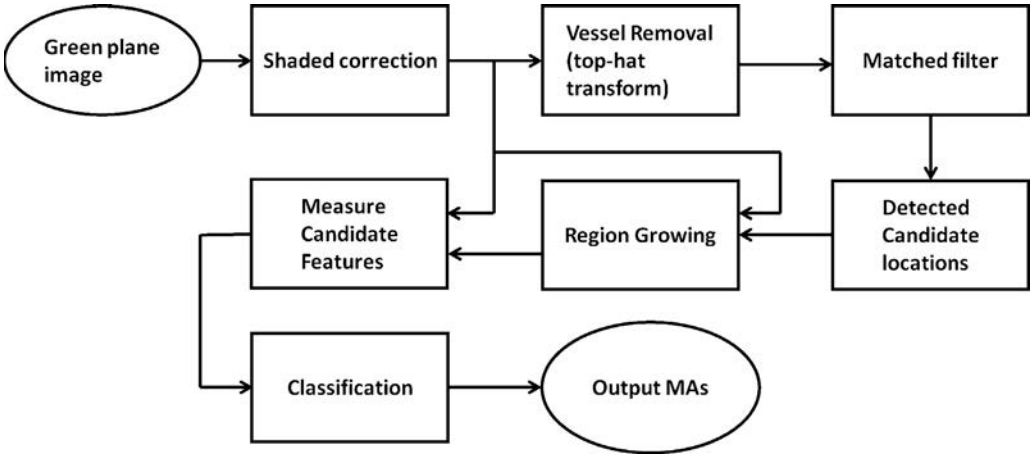

Fig. 1. Schematic of the "standard" approach to microaneurysm detection.
Adapted from [1]

This paper is organized as follows. Section 2 consists of a literature review of MA detection in color fundus images. Section 3 describes the proposed approach and its two main phases (preprocessing and the MAS model). The results are shown and discussed in Section 4. Finally, Section 5 presents the conclusion and some proposals for future research.

2. Related studies

Several approaches have previously been proposed with regard to MA segmentation through fundus image analysis. These approaches are frequently based on morphological [5,6], template-matched [7–9] and supervised learning methods [10,11]. The supervised methods are frequently preceded by one of the two other approaches [5,6,9].

Some previous approaches have examined the detection of MAs in fluorescein angiographies. In this type of image, MAs appear as bright patterns and with improved contrast, compared to the green plane image from the RGB color space. However, MAs have some characteristics in common in both images; they appear small, isolated and of a circular shape, which is fundamental when using morphological approaches. The first algorithm was developed by Laÿ [12] and then improved by other authors [6,10,13]. These approaches utilized the top-hat transformation to discriminate between circular, non-connected, red lesions and the elongated vasculature. The method consists of morphological opening of the green channel images, with a linear structuring element at different orientations to obtain the vasculature, and then removing it from the original image. The length of the structuring element is chosen to be sufficiently short to fit inside curved vessels, and long enough that it cannot fit inside MAs, such that it detects vessels (and other large extended features), but not MAs. However, if the length of the structuring element is increased to allow detection of larger objects, vessel segmentation deteriorates, leading to the detection of a greater number of spurious candidate objects on the vessel. This approach has been modified and subsequently used by other authors, such as Walter et al. [5], who detected MA candidates by applying diameter closing and an automatic threshold scheme.

Niemeijer et al. [10] developed an MA detection approach that has since inspired several research groups [6,13], and this is schematically illustrated in Fig. 1. First, the digital green plane image is shade-corrected to make uniform the background illumination of the retinal images. Shade-correction is normally achieved by estimating the background illumination image by means of a large median or mean filtering. The background image is either subtracted from, or divided by, the green plane image. The next step consists of detecting the vasculature by morphologically opening the shade-corrected image with a linear structuring element at several angles, to enhance all vessel segments (top-hat transformation). The segmented vessels are then subtracted from the shade-corrected image. The resulting image contains small, dark objects, such as MAs, and small fragments left over from the vessels, which are then highlighted by applying a matched-filter with a circularly symmetric 2D Gaussian as a kernel. Hereafter, the image is thresholded to detect the candidate MAs, which will be used as locations to initiate a region-growing process on the shade-corrected image to delineate the underlying morphology of the candidate. Finally, intensity and shape descriptors are determined in the region-grown object and a classifier used to ameliorate MA detection. The primary drawback of this approach is that it cannot typically detect MAs close to vessels.

Zhang et al. [8] presented an approach that differed from the "standard" in the way that the MA candidates and vessels were detected. Using this method to detect candidates, a non-linear filter with five Gaussian kernels with different standard deviations was applied to the input retinal images. By maintaining the maximal correlation coefficient for each pixel, a maximal correlation response image was obtained, which was then thresholded with a fixed threshold value to determine the candidates. The vessels were segmented by an adaptive thresholding technique and then used to reduce the number of candidates. Finally, the region-growing process was applied to determine the precise size of all candidates, and a set of features was extracted for each. The same research group [9] recently improved their method by including a supervised classifier at the final stage, which was the dictionary learning with sparse representation.

The approach used by Sánchez et al. [11] began with a normalization process identical to the standard approach. An unsupervised mixture-model-based clustering method was then used to extract candidates on the normalized image intensities. A fitted model was obtained by fitting a Gaussian mixture model to the image intensities. The MAs candidates were segmented by applying a threshold to the fitted model. After automatically masking out the vasculature, a set of color, shape and texture features were extracted from the remaining candidates for use in a logistic regression, to determine the likelihood of their being MAs.

Mizutani et al. [14] tailored their approach by applying brightness correction, gamma correction and contrast enhancement, in order to normalize the intensity and contrast between images. The extraction of MA candidates was performed using a modified

Table 1
Results and methodology categories of ROC approaches.

Publication	Team name	Method category	Final score
Cree [13]	Waikato	Morphology and template matching for segmentation and a supervised classification	0.206
Mizutani et al. [14]	Fujita	Supervised	0.310
Sánchez et al. [11]	GIB Valladolid	Supervised	0.322
Zhang et al. [8]	OKMedical	Template matching	0.357
Zhang et al. [9]	OKMedical_II	Template matching and supervised	0.369
Giancardo et al. [15]	ISMV	Template matching and supervised	0.375
Quellec et al. [7]	LaTIM	Template matching	0.381
Niemeijer et al. [10]	Niemeijer et al.	Morphology and template matching for segmentation and a supervised classification	0.395
Lazar et al. [16]	Lazar et al.	Morphology and template matching	0.423
Antal and Hajdu [17]	DRSCREEN	Supervised	0.434

double ring. The original double ring filter detects regions in the image in which the average pixel value is lower than the average pixel value in the region surrounding it. Conversely, in order to reduce spurious detections on small capillaries, the modified filter designed by the authors detects regions where the average pixel value in the surrounding region is lower by a certain fraction of the number of pixels under the filter. Hereafter, the original double ring filter with a different parameter setting was used to detect the vasculature and so to remove false positive candidates that remained. The region-growing process was then performed and a set of features, based on color, intensity, shape, and contrast, were extracted for use as input to an artificial neural network.

After normalizing the images using the standard approach, Giancardo et al. [15] selected as MA candidates the pixels with an intensity value higher than a specific threshold. Consequently, the Radon transformation was calculated at various scanning angles on original image windows for which at least one MA candidate existed. The result of this step was a set of features that was classified through principal component analysis and support vector machines.

Quellec et al. [7] proposed a method based on template matching in the wavelet domain to detect MAs. In this domain, without other image processing, it was possible to overcome the problems caused by lighting variations or high-frequency noise by choosing the working sub-bands. The authors sought the wavelet basis that was best able to discriminate between lesions and lesion-free areas. The MAs were modeled with 2D rotation-symmetric generalized Gaussian functions, and the wavelet basis was designed empirically, by a numerical optimization procedure, using the lifting scheme framework.

Lazar and Hajdu [16] presented an approach whereby cross-section profiles with multiple orientations were used to construct a multi-directional height map, in which each pixel contained a set of height values that represented the difference between the pixel and its surroundings in a particular direction. A score map resulted from the application of a modified multilevel attribute opening step on the height map. The small, dark circular, objects had the highest scores on this map, so the MAs could be extracted by thresholding. Antal and Hajdu [17] proposed an ensemble-based framework to select the optimum combination between the preprocessing methods and MA candidate extractors that had previously been described.

With regard to the detection of MAs in color fundus images, Niemeijer et al. [18] created the Retinopathy Online Challenge (ROC) website. Its aim is to bring together research community efforts toward the creation of algorithms for the detection of MAs, by evaluating their performance on a common dataset and with the same evaluation modality. This permits a fair comparison between algorithms of different groups. To date, 11 research groups have displayed their results on the website. The methodologies they used, which have been published, are all described above, and the results are shown in Table 1.

3. Materials and methods

3.1. Multi-agent paradigm

The primary goal of MAS research is to find methods that allow the building of complex systems composed of multiple autonomous entities, called agents, which, while operating on local knowledge and possessing only limited abilities, are nonetheless capable of enacting the desired global behaviors. A MAS is generally composed of a set of agents situated in a virtual or real environment. The agents interact with each other to coordinate their behavior in a particular organization that can be dynamic and/or self-adaptive. The self-adaptation results from the agents' interaction to adapt themselves to the environment and its constraints. The differentiation of the agents and their interaction allow the emergence of a global result, which influences the agents of the system, making them converge toward a common, often unexpected solution, which is not understood at the individual level. The dynamic results from an emergent phenomenon allow additional functionality that each agent cannot provide individually.

This study aimed to develop a MAS model for MA segmentation in fundus images. To prepare the environment in which the agents will be situated, and will interact, a group of conventional image-processing algorithms were implemented in a first phase (image preprocessing). An overall view of the proposed approach is illustrated in Fig. 2.

3.2. Environment – image preprocessing

We chose the green plane image to prepare the information (environment) for the MAS model, since this is the plane in which MAs have the highest contrast with the surrounding background. First, an estimated background image was obtained by means of a large median filter applied to the green image. This image was then subtracted from the original green image, resulting in a shaded corrected image with no background intensity variation across it, and with the bright structures eliminated. MAs reveal a Gaussian shape, so a Gaussian filter (width = 3; $\sigma = 1$) was then applied to enhance the small, dark structures. The final step of this phase consisted of applying a modified Kirsch filter [19] to obtain edges of a two-pixel thickness (Fig. 3). This enables the MAS model detection process, since MAs present specific gradient patterns, some examples of which can be observed in Fig. 3c.

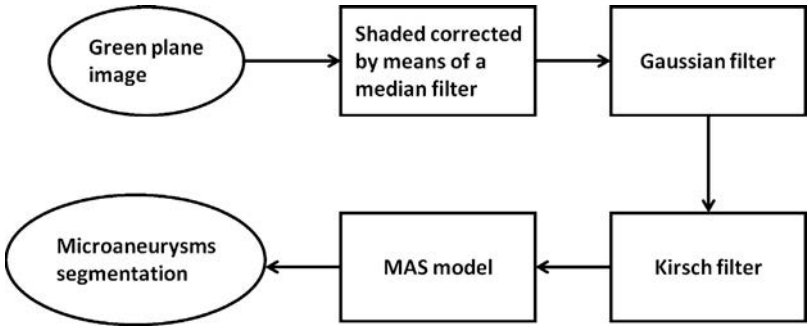

Fig. 2. Schematic representation of the proposed approach.

3.3. Model overview

The system is composed of a set of reactive agents, which are dynamically launched and destroyed without external control. The agents have the ability to extract the information they need from the environment, and to autonomously act on it. Therefore, each agent has the appropriate sensors and behaviors, as well as influences (reactions) over the environment, to perform the tasks for which it was designed. The sensors permit the agents to perceive information from the environment, and, according to the perceptions returned, agents act by sending influences to the system (agents or environment). The influences form part of a behavior and are all the actions an agent can carry out. The environment encompasses the prepared information (input images), its characteristics, and the results.

The segmentation and exploration of the image are commanded by the behaviors of the agent. Each behavior may comprise several tasks, according to the agent state, which can be changed by itself, responding to the system conditions, or by another agent. There are two types of agents, defined by their perception and current state: explore agents (EAs) and region agents (RAs).

An overview of the proposed MAS model algorithm is illustrated in Fig. 4. The EA explores the environment and launches an RA when it finds a region of interest. The RA then segments and analyzes its region. In addition, RAs negotiate with each other to attempt fusion of regions. The next subsections detail the algorithm that was implemented to allow agents to segment all the small and isolated dark structures in fundus images.

3.4. Algorithm description

Each pixel of the environment contains the intensity gray level, as well as a Boolean value defining whether the pixel has already been explored by an agent. Furthermore, when located in the environment, the agents perceive the modified Kirsch gradient.

The sensors, behaviors, and respective states, as well as the influences for each type of agent defined in this algorithm are described in Table 2. The details of each behavior are illustrated in Figs. 5 and 6.

The MAS model is initialized with an EA in the "active" state, launched on one randomly chosen white point from Fig. 3b. It evolves in the environment by analyzing positive gradient points and their neighbors to seek specific gradient patterns corresponding to MAs. When a valid pattern is found, the EA launches an RA and becomes "inactive". This RA is at the "explore" state, in which it follows an edge until there is no direction to follow. The RA then modifies its own state to "waiting" and sends a message to the EA to change its state to "active". This process is repeated until all the positive gradient points have been explored by agents. The EA then sends a message to all RAs to modify their state to "fusion", in which they attempt to fuse with their RA neighbors by sending messages to them. An RA treats another RA as a neighbor if the distance between at least one of its points and one point of the other RA is smaller or equal to a specific threshold (D). The two neighbor RAs are then replaced by a new RA that contains the information of the merged regions.

Each RA then determines its region contour size and if it is smaller than a threshold (T_c), it fills the region, accounting for the image gray-level values, otherwise, the RA disappears

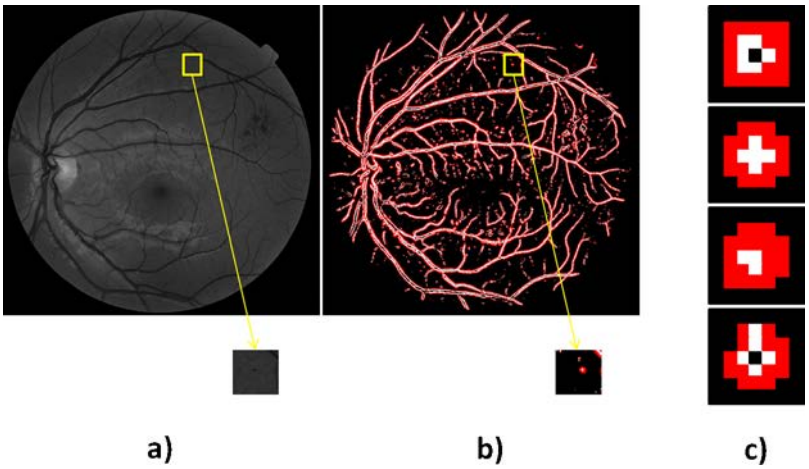

Fig. 3. (a) Green plane image; (b) modified kirsch filter resulting image where the red and white pixels represent negative and positive values, respectively; (c) characteristic gradient pattern of microaneurysms. (For interpretation of the references to color in this figure legend, the reader is referred to the web version of this article.)

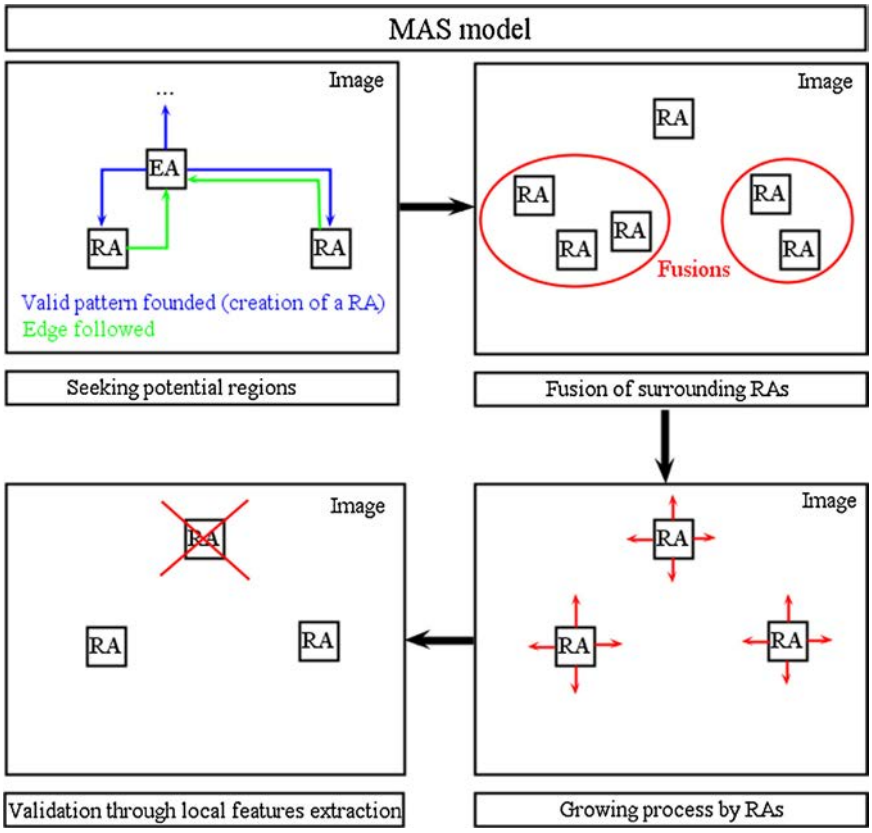

Fig. 4. Schematic representation of the proposed multi-agent system model.

Table 2
Summary of agents' sensor, behavior and influences in the proposed MAS model.

Agent	Sensors	Behavior and states	Reactions
Explore agent	Current position Gradient corresponding to its current position and neighbors Positive gradient points list (Lp)	Explore behavior Active Inactive	Remove the explored point from the list Lp Add RA Send and receive messages Change RA state
Region agent	Current position Its points list Gradient corresponding to its current position and neighbors Gray level intensity corresponding to its current position and neighbors	Region Behavior Explore Waiting Fusion Filling	Add RA Send and receive messages Change EA state

with its region. Hereafter, each RA performs a region-growing to ensure that remaining candidates represent the true MA size. Finally, the RA analyzes its region shape and intensity profile to validate it as a true lesion. At the end of the process, agents should segment all the small and isolated dark structures.

Several steps referred to above must be addressed to better understand the MAS model algorithm proposed here. These are described in the following sub-sections.

3.4.1. *Seeking potential regions*

When evolving in the environment, the EA looks for small, dark structures by checking whether the pixel in which it is located verifies these conditions: (1) it has not yet been visited by another agent; and (2) it corresponds to the MA pattern. To verify the second condition, the agent analyzes gradient profiles in the neighborhood in four directions (Fig. 7a). If it discovers the sequences negative–positive–null–positive–negative or negative–positive–negative gradient values in at least two

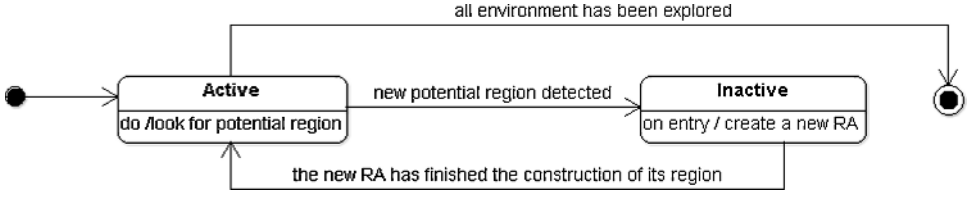

Fig. 5. UML state diagram of the explore behavior.

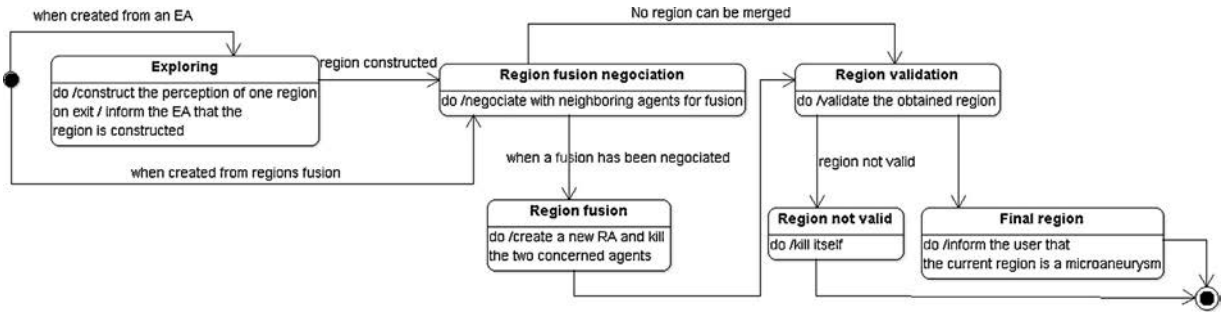

Fig. 6. UML state diagram of the region behavior.

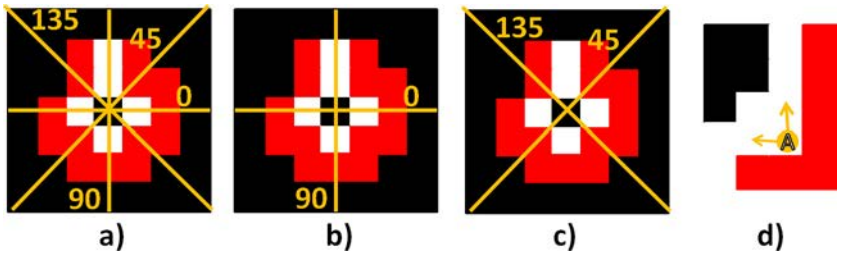

Fig. 7. Representation of the explore behavior (a–c); (d) possible directions to follow, according to region agent restrictions.

perpendicular directions (Fig. 7b and c), it views the pixel as belonging to a dark structure. If the agent cannot confirm one of the two conditions it moves to another, randomly chosen, point with positive gradient.

3.4.2. Directions to follow

Agents search for the white points in their 8-neighborhood that have a red point in the 4-neighborhood, in order to determine possible directions to follow. This red point must also belong to the 8-neighbors of the target pixel. For instance, in Fig. 7d, only two directions are available.

3.4.3. Region filling

The region is filled by analyzing the gray level points located between each pair of boundary points, for which a line equation that contains the two points is calculated (Fig. 8a and b), and the points located between them are determined. An evaluation related to its gray level intensity is made for each of them. The point is added to the region if its gray level value is lower than the average of the gray level values of the points that are already in the region (Fig. 8c).

3.4.4. Region growing

The RA performs a region-growing algorithm based on [10]. This algorithm determines the threshold by $t = I_{\text{darkest}} - \alpha(I_{\text{darkest}} - I_{\text{bg}})$, where I_{darkest} is the candidate with the lowest intensity pixel in the green plane image, I_{bg} is the corresponding intensity in the background image, and α is set to 0.5 [10]. The growing process stops when there are no more pixels in the 8-neighborhood with an intensity lower than the threshold, or when the region size is bigger than a threshold ($A_{\max}$).

3.4.5. Region validation

The RA validates its region as a true lesion by means of shape- and intensity-based features analysis. For region-shape analysis, the RA calculates elongation, since some detected regions belong to thin blood vessel fragments, meaning they have higher elongation values. Since MAs are round local minimums, they can be represented as an inverted 2D Gaussian shape. Therefore, a set of cross-sectional intensity profiles was obtained from the inverted green channel for the region intensity analysis (Fig. 9). To determine these profiles, a window around the region was considered. The region was then dilated for use as a mask on the inverted green plane, where scanning lines 15° rotated were applied. From these 12 intensity profiles, the Gaussian fitting parameters (height of the Gaussian peak – a, position of the center of the peak – b, width of the Gaussian "bell' – c) (Fig. 9 below) were determined and analyzed (Table 3) for all regions of several images. Analyzing Table 3, we may notice that parameter *c* allowed a better discrimination between small, red lesions and other dark structures. In that way, the difference between the maximum and the minimum parameter *c* values of the 12 profiles was maintained as an intensity-based feature (*c_range*).

The features value used by the RA to evaluate its region were *elongation* $\in \{1 : 0.2 : 4\}$ and *c_range* $\in \{0 : 1 : 20\}$.

3.5. Retinal images and system performance evaluation

A set of images by Quellec et al., available online [7] and called LaTIM (Laboratoire de Traitement de l'Information Médicale) dataset in this study, was used for the performance evaluation. This dataset consisted of 36 images with 2240×1488 pixels and was stored in tiff file format. Moreover, the dataset also contained a text file for each image, with small, red lesions manually annotated by a single DR expert.

Another publicly available database used in this study was provided in the ROC competition [18]. This database was composed of 100 images, equally divided into a training set and a test set. The images were acquired by three different cameras and were of

Table 3
Gaussian fitting parameters (a, b and c).

	Small red lesion			Other		
	a	b	c	a	b	c
Minimum	0.676	2.730	7.50	0.538	2.740	5.560
Maximum	0.829	5.209	16.553	0.817	9.102	185.262
Mean	0.742	3.856	11.147	0.700	4.482	17.854
Standard deviation	0.038	0.479	1.856	0.053	0.904	9.567

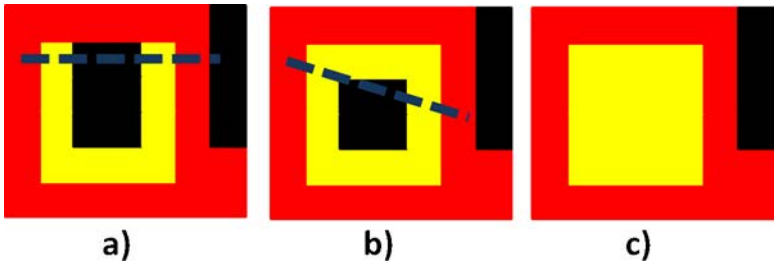

Fig. 8. Region agent "filling" state graphical representation.

different resolutions and sizes, ranging from 768×576 to 1389×1383. All images were stored in JPEG format, and compression was set in the camera. All MAs and other irrelevant lesions from the 100 images were annotated by four retinal experts. The irrelevant lesions were objects that, despite not being MAs, may be identified as such by an automated program. For instance, hemorrhages and pigment spots are similar in appearance to MAs, so they should not be considered as false positives. For the training set, the lesion locations annotated by the four experts were combined by a logical OR, while for the test set, the reference standard was obtained in a different way. The annotations of one randomly chosen expert were kept for human observer performance use. The lesions annotated by the other three experts were combined for the final reference standard, in which "MA" was an object that was labeled as such by at least two experts. Those lesions identified by only one specialist were assigned as "irrelevant".

For both datasets, the proposed approach performance was evaluated in terms of the free-response receiver-operating characteristic (FROC) curve, where per lesion sensitivity values were plotted against the average number of false positives (FP) per image. Sensitivity represents the proportion of MAs correctly detected by the algorithm, while FP is the number of non-MAs identified as MAs. For the ROC dataset, and to facilitate the comparison with the other methods already submitted on the challenge website, the FROC curve was summarized in several quantitative points, by which method the sensitivity values for the false positive per image rates values of (1/8), (1/4), (1/2), 1, 2, 4, and 8 were achieved and averaged to obtain a final score. Moreover, only the results obtained with the test set and provided by the ROC organizers were analyzed, as described in the next section.

4. Results

To facilitate the algorithm parameterization, the sizes of all images from both datasets were normalized without losing the relevant study information. The LaTIM images were resized to 1120×744 pixels and the ROC images to 836×835 pixels. The algorithm parameters were chosen according to the image size and the typical dimension of MAs in fundus images, thereby $T_c = 40$, $D = 2$ and $A_{\max} = 40$ were the values used when applying the proposed approach to both datasets.

The MAS model performance depended on the preprocessing step and how the agents interpreted the information provided from this first phase. As such, it is important to compare the

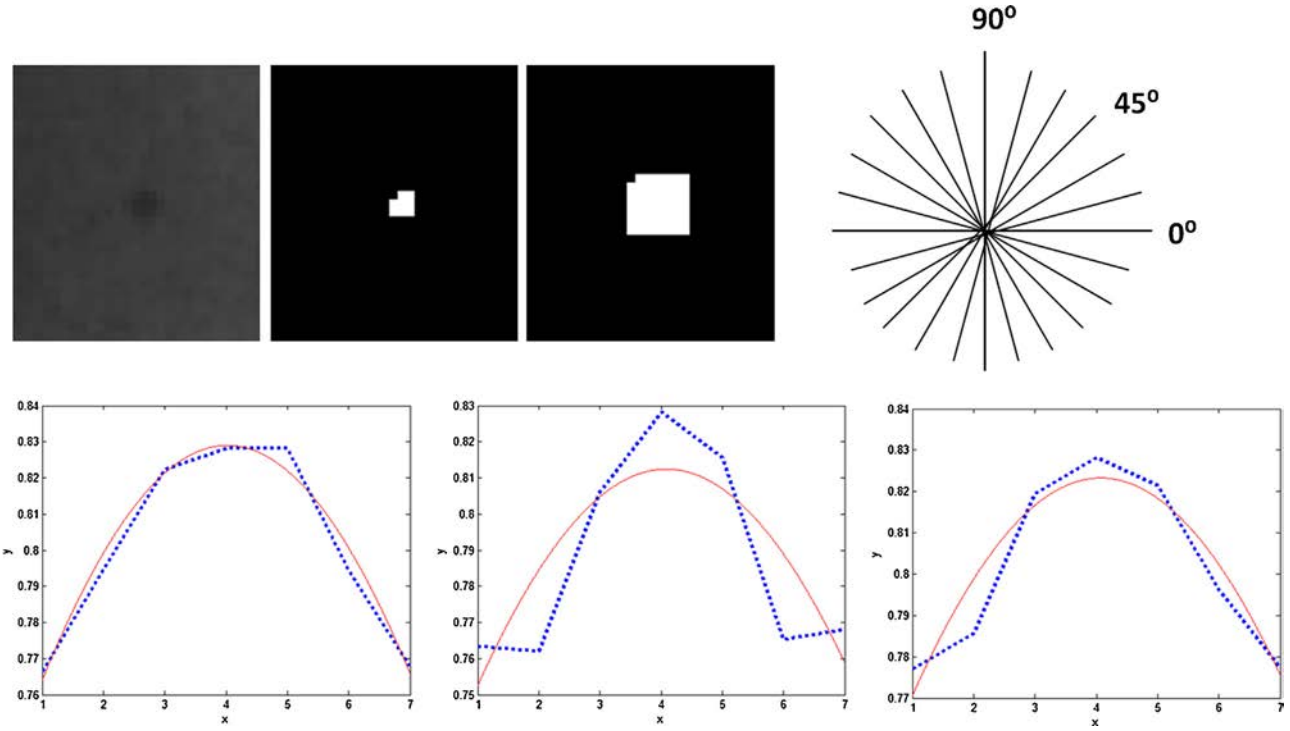

Fig. 9. Above (from left to right): window of the green plane image centered at a microaneurysm; window of the binary candidates image with a microaneurysm candidate; the candidate of the previous image after a dilation; scan lines to be performed on the inverted green plane with the aid of mask from previous image. Below: microaneurysm intensity profiles (dotted blue line) and respective Gaussian fitting function (red line) for orientations 0°, 90° and 135°. (For interpretation of the references to color in this figure legend, the reader is referred to the web version of this article.)

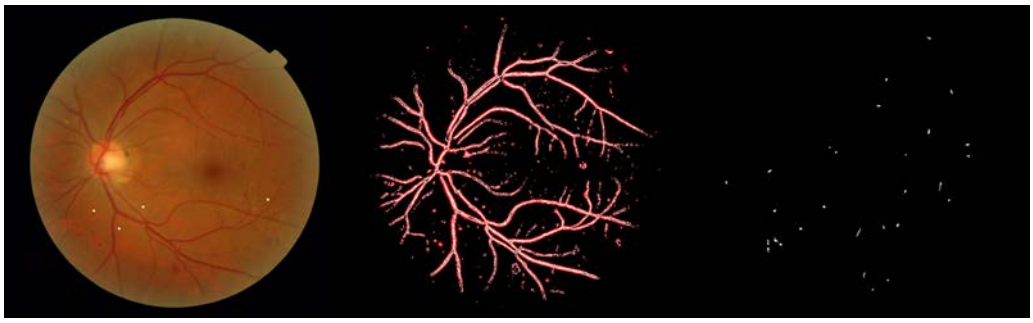

Fig. 10. From left to right: manually annotated microaneurysm superimposed with the original image; image resulting from the preprocessing phase; segmentation performed by the multi-agent system model before local feature extraction and analysis.

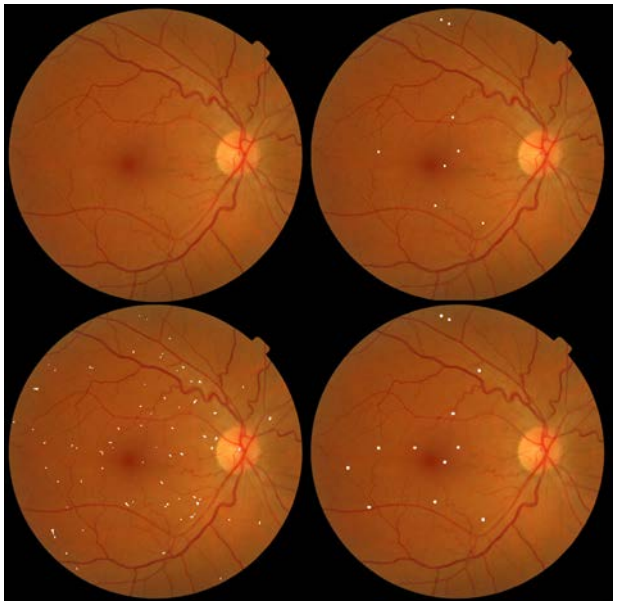

Fig. 11. Images resulting from the proposed approach. Above (from left to right): color image; binary image with manually annotated microaneurysm superimposed with color image. Below (from left to right): binary image with candidates detected by the multi-agent system model before feature analysis and superimposed with color image; binary image resulting from local feature analysis superimposed with color image.

gradient image resulting from the preprocessing step with the binary image resulting from the MAS model. Fig. 10 illustrates an original color image with manually segmented MAs and the respective image resulting from the preprocessing phase, and the binary image provided by the MAS model before the local feature analysis. Fig. 11 demonstrates the binary images that resulted from the MAS model before and after the feature analysis step, made by the RAs. The segmentation performance obtained with the MAS model in the LaTIM dataset was compared with another approach, which is schematically illustrated in Fig. 12 (bold), and consists of the preprocessing and segmentation phases of the "standard" approach referred in Section 2. That is, only the detection method of the candidate was considered because the proposed approach is unsupervised and, in that way, a fair comparison is made. The comparative results are illustrated in Fig. 13 where the curve for the "standard" approach was obtained by varying the threshold value ($t \in \{3 : 1 : 12\}$). Fig. 14 shows the results related to the detection of MAs close to blood vessels using the two approaches.

Fig. 15 and Table 4 demonstrate the FROC curves and the ranked quantitative results, respectively, of the ROC methods already described in Section 2. The final score of the proposed approach is 0.240, which corresponds to 10th place in the competition.

5. Discussion

Fig. 10 shows that the MAS model is capable of detecting small, dark structures and excludes most of the edge pixels belonging to blood vessels and some artifacts. In fact, all of the four MAs were correctly segmented and the remaining elongated structures could be easily removed with the local feature analysis step. Fig. 11 shows a false positive sensitivity of 1 and 4, representing a very good performance, considering only two features of the candidates. Therefore, it seems that the inclusion of an agent-based learning classifier at the final stage should improve the algorithm performance.

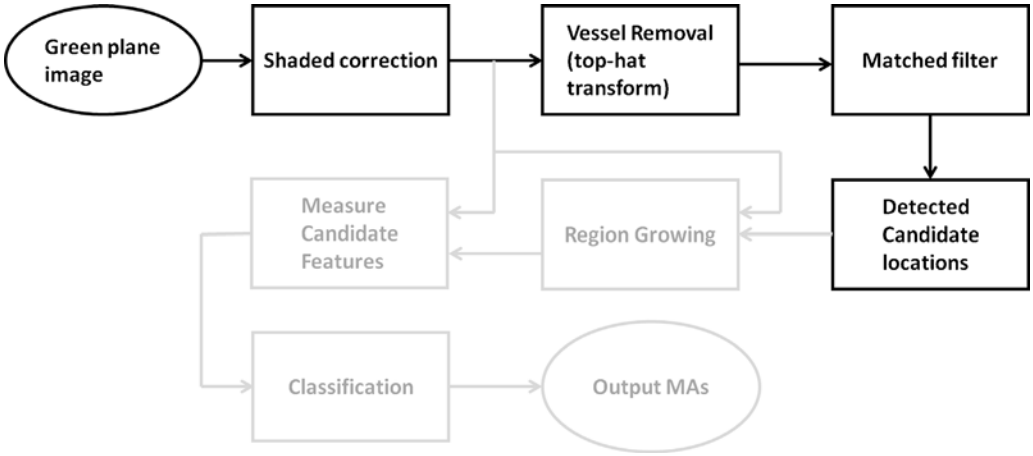

Fig. 12. Schematic representation of a classical approach used for microaneurysm segmentation.

Table 4
Sensitivities of different approaches at various false positive points for the ROC test dataset.

Author	1/8	1/4	1/2	1	2	4	8	Final score
Waikato	0.055	0.111	0.184	0.213	0.251	0.3	0.329	0.206
Our approach	0.053	0.083	0.135	0.187	0.276	0.407	0.540	0.240
Fujita	0.181	0.224	0.259	0.289	0.347	0.402	0.466	0.310
GIB Valladolid	0.19	0.216	0.254	0.3	0.364	0.411	0.519	0.322
OKMedical	0.198	0.265	0.315	0.356	0.394	0.466	0.501	0.357
OKMedical_II	0.175	0.242	0.297	0.370	0.437	0.493	0.569	0.369
ISMV	0.217	0.270	0.366	0.407	0.440	0.459	0.468	0.375
LaTIM	0.166	0.23	0.318	0.385	0.434	0.534	0.598	0.381
Niemeijer et al.	0.243	0.297	0.336	0.397	0.454	0.498	0.542	0.395
Lazar et al.	0.251	0.312	0.350	0.417	0.472	0.542	0.615	0.423
DRSCREEN	0.173	0.275	0.380	0.444	0.526	0.599	0.643	0.434

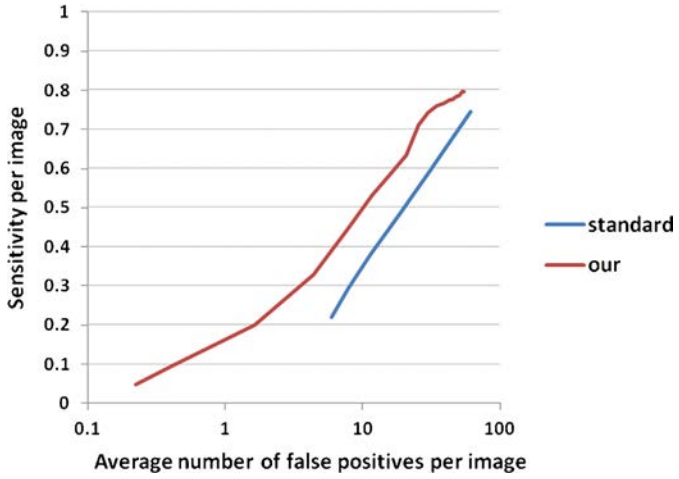

Fig. 13. FROC curves obtained with the proposed and "standard" approaches applied to the LaTIM dataset.

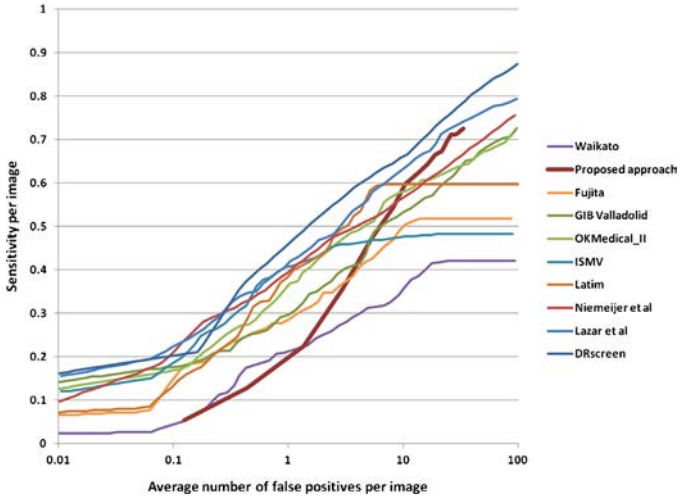

Fig. 15. FROC curves of the ROC methods.

Fig. 13 shows that our approach clearly outperformed the "standard" approach. For any value of the average number of false positives, it always produced a higher sensitivity value, meaning that our method detects a greater number of candidates that are true MAs than does the "standard" approach. A careful analysis of images resulting from the two approaches reveals that ours has the advantage of preserving MAs close to vessels (Fig. 14). This is very important for clinical practice, since this type of lesion very often appears close to vessels.

The inclusion of this approach in the ROC gave relevance to the present study, since it can be fairly compared to other previously

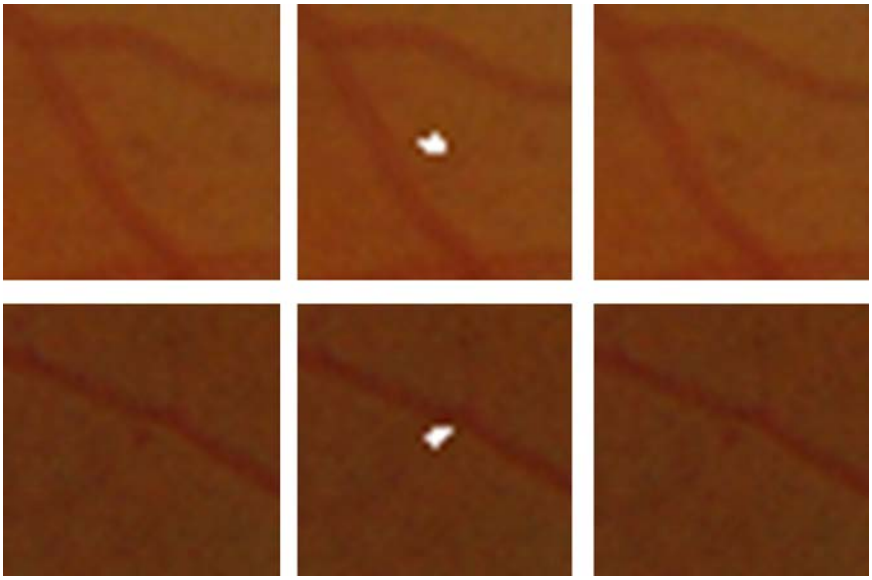

Fig. 14. Comparative results related to the detection of microaneurysms close to blood vessels. From left to right: original color image; multi-agent system model result; "standard" approach result.

reported methods. With a final score of 0.240, our results are encouraging, in that they are comparable with the other ROC methods. The FROC curve of the proposed approach (Fig. 15) and the quantitative results shown in Table 4 show that for an average number of FP of 8, the sensitivity value was higher than 0.5, representing an improved performance, compared to other methods. In fact, only the DRscreen approach and that used by Lazar et al. gave higher sensitivity values at this average number of FP. Therefore, it seems that there are some issues with our MAS model, with regard to discriminating between the candidates that are true small, red lesions and those that are false positive, which may be a problem of the local validation step. Therefore, other features should be evaluated. Moreover, the use of further agent potential, such as learning capacities, should allow the integration of some knowledge regarding the particularities of the retina. The combination of this approach with methods to segment other important retinal structures could also improve system performance.

6. Conclusions

A new, small, red-lesion segmentation algorithm, based on a MAS approach, was proposed in this study. Through agent local interaction, the improvement of traditional algorithm results was possible, primarily by the detection of MAs close to vessels. The addition of a validation step through a local feature analysis allowed the reduction of the average number of FP and encourages the inclusion of some agent learning capacity for future improvement of the algorithm. The comparison with the ROC methods was important for showing the scientific impact of the proposed approach. Indeed, despite not being optimum, our results are encouraging and can be compared with those that have previously been reported.

Overall, the results show that the use of a MAS model at the micro level could be an effective way to segment red lesions in fundus images, and to overcome some common problems that have previously been reported, such as the detection of MAs close to vessels. In future, the MAS model should be improved to embrace some agent-learning capacities, as well as some knowledge regarding retina geometry and other particularities.

Acknowledgments

Work supported by FEDER funds through the "Programa Operacional Factores de Competitividade – COMPETE" and by national funds by FCT – Fundação para a Ciência e a Tecnologia. C. Pereira thanks the FCT for the SFRH/BD/61829/2009 grant. The authors also would like to thank to the reviewers for their valuable comments for this article improvement.

References

[1] Cree MJ. Automated microaneurysm detection for screening. In: Jelinek HF, Cree MJ, editors. Automated image detection of retinal pathology. Boca Raton, FL: CRC Press; 2010. p. 155–84.
[2] Richard N, Dojat M, Garbay C. Automated segmentation of human brain MR images using a multi-agent approach. Artificial Intelligence in Medicine 2004;30(2):153–76.
[3] Bovenkamp E, Dijkstra J, Bosch J, Reiber J. Multi-agent segmentation of IVUS images. Pattern Recognition 2004;37(4):647–63.
[4] Pereira C, Mahdjoub J, Guessoum Z, Gonçalves L, Ferreira M. Using MAS to detect retinal blood vessels. In: Pérez JB, Rodríguez JM, Adam E, Ortega A, Moreno MN, Navarro E, et al., editors. Highlights on practical applications of agents and multi-agent systems; vol. 156 of advances in intelligent and soft computing. Berlin, Heidelberg: Springer-Verlag; 2012. p. 239–46.
[5] Walter T, Massin P, Erginay A, Ordonez R, Jeulin C, Klein J. Automatic detection of microaneurysms in color fundus images. Medical Image Analysis 2007;11(6):555–66.
[6] Fleming A, Philip S, Goatman K, Olson J, Sharp P. Automated microaneurysm detection using local contrast normalization and local vessel detection. IEEE Transactions on Medical Imaging 2006;25(9):1223–30.
[7] Quellec G, Lamard M, Josselin P, Cazuguel G, Cochener B, Roux C. Optimal wavelet transform for the detection of microaneurysms in retina photographs. IEEE Transactions on Medical Imaging 2008;27(9):1230–41.
[8] Zhang B, Wu X, You J, Li Q, Karray F. Detection of microaneurysms using multi-scale correlation coefficients. Pattern Recognition 2010;43(6):2237–48.
[9] Zhang B, Karray F, Li Q, Zhang L. Sparse representation classifier for microaneurysm detection and retinal blood vessel extraction. Information Sciences 2012;200:78–90.
[10] Niemeijer M, van Ginneken B, Staal J, Suttorp-Schulten M, Abràmoff M. Automatic detection of red lesions in digital color fundus photographs. IEEE Transactions on Medical Imaging 2005;24(5):584–92.
[11] Sánchez C, Hornero R, Mayo A, García M. Mixture model-based clustering and logistic regression for automatic detection of microaneurysms in retinal images. In: Karssemeijer N, Giger ML, editors. SPIE medical imaging 2009: computer-aided diagnosis. International Society for Optics and Photonics; 2009. p. 72 601M.
[12] Laÿ B [thesis doctoralis] Analyse automatique des images angiofluorographiques au cours de la rétinopathie diabétique. Paris, France: School of Mines; 1983.
[13] Cree M [Online] The waikato microaneurysm detector, Technical Report. Hamilton, New Zealand: University of Waikato; 2008. p. 4. Available from: http://roc.healthcare.uiowa.edu/results/documentation/waikato.pdf
[14] Mizutani A, Muramatsu C, Hatanaka Y, Suemori S, Hara T, Fujita H. Automated microaneurysm detection method based on double ring filter in retinal fundus images. In: Karssemeijer N, Giger ML, editors. SPIE medical imaging 2009: computer-aided diagnosis. International Society for Optics and Photonics; 2009. p. 72 601M.
[15] Giancardo L, Meriaudeau F, Karnowski T, Li Y, Tobin K, Chaum E. Microaneurysm detection with radon transform-based classification on retina images. In: 2011 annual international conference of the IEEE engineering in medicine and biology society, EMBC, IEEE. 2011. p. 5939–42.
[16] Lazar I, Hajdu A. Microaneurysm detection in retinal images using a rotating cross-section based model. In: IEEE international symposium on biomedical imaging: from nano to macro. 2011. p. 1405–9.
[17] Antal B, Hajdu A. An ensemble-based system for microaneurysm detection and diabetic retinopathy grading. IEEE Transactions on Biomedical Engineering 2012;59(6):1720–6.
[18] Niemeijer M, van Ginneken B, Cree MJ, Mizutani A, Quellec G, Sánchez C, et al. Retinopathy online challenge: automatic detection of microaneurysms in digital color fundus photographs. IEEE Transactions on Medical Imaging 2010;29(1):185–95.
[19] Mahdjoub J [thesis doctoralis] Vers un système de vision auto-adaptatif à base de systems multi-agents. Reims, France: Université Reims Champagne-Ardenne; 2011.